 CMES, vol.87, no.5, pp.387-409, 2012

Effects of the Axial Variations of Porosity and Mineralization on the Elastic Properties of the Human Femoral Neck

V. Sansalone[1,*], V. Bousson[2], S. Naili[1], C. Bergot[2], F. Peyrin[3] J.D. Laredo[2] and G. Haïat[1]

Abstract: This paper investigates the effects of the heterogeneous distribution of the Haversian Porosity (HP) and Tissue Mineral Density (TMD) on the elastic coefficients of bone in the human femoral neck. A bone specimen from the inferior femoral neck was obtained from a patient undergoing standard hemiarthroplasty. The specimen was imaged using 3-D synchrotron micro-computed tomography (voxel size of 10.13 μm), leading to the determination of the anatomical distributions of HP and TMD. These experimental data were used to estimate the elastic coefficients of the bone using a three-step homogenization model based on continuum micromechanics: (i) At the tissue scale (characteristic length of several hundred micrometers), bone was modeled as cylindrical pores (Haversian canals) in a solid matrix called ultrastructure; (ii) At the scale of several micrometers, ultrastructure was modeled as collagen fibers embedded in a mineral foam; (iii) Eventually, at the scale of several hundred nanometers, mineral foam was modeled as a mixture of mineral and water. Effective elastic coefficients of the bone were computed accounting for the heterogeneous distributions of HP and TMD determined experimentally. The variations of HP, TMD and elastic coefficients were investigated along the axis of the femoral neck and at different distances from the periosteal surface of the sample. TMD was found to decrease from the distal to the proximal part of the femoral neck axis whereas no specific trend was found for the HP. Axial variations of the elastic coefficients were shown to be mainly related to the axial variations of TMD and HP in the dense and porous tissue, respectively. Therefore, this study underlines the importance of considering the actual spatial

[1] Université Paris-Est, Laboratoire Modélisation et Simulation Multi Echelle, UMR CNRS 8208 MSME, 94010 Créteil Cedex, France.

[2] Université Paris Diderot, Sorbonne Paris Cité, UMR CNRS 7052 B2OA, 10, avenue de Verdun, 75010 Paris, France.

[3] CREATIS, INSERM U630; UMR CNRS 5220; INSA Lyon; Université de Lyon, 69621 Villeurbanne, Cedex, France. ESRF, BP 220, 38043 Grenoble, Cedex, France.

variations of TMD and HP to obtain accurate estimates of bone effective elastic properties.

Keywords: Biomechanics, bone, femoral neck, haversian porosity, tissue mineral density, imaging, homogenization, elastic properties.

1 Introduction

Bone is a complex material coupling stiffness, strength and lightweight. These amazing mechanical properties are mainly due to the hierarchical structure of bone spanning several length scales, from the organ to the atomic scale. Bone structure is different according to the animal species, age, gender, health state and anatomical site. Bone is continuously remodeled by bone cells to adapt its structure to the prevailing mechanical and biochemical environment. Abnormal remodeling is often related to bone diseases such as osteoporosis. For osteoporotic patients, bone mass is lost with a substantial weakening of the bone mechanical properties and increased risk of fracture. In the femoral neck, osteoporotic bone structure is characterized by progressive thinning of the outer cortical shell and loss of trabecular mass [Mayhew, Thomas, Clement, Loveridge, Beck, Bonfield, Burgoyne, and Reeve (2005)]. Hip fracture risk depends on the quality of both cortical and trabecular bone tissues which both contribute to bone stiffness and toughness [Manske, Liu-Ambrose, Cooper, Kontulainen, Guy, Forster, and McKay (2008)]. Cortical bone in the femoral neck region supports most of the stresses associated with normal gait [Lotz, Cheal, and Hayes (1995)]. Therefore, effective mechanical properties of the cortical bone are an important determinant of the hip fracture risk. The amount of bone tissue given by bone mineral density (BMD) at the hip as measured with Dual X-ray absorptiometry has long been considered as a surrogate marker of bone strength. However, BMD remains unable to estimate bone quality, which is intrinsically a mechanical property depending on bone composition and microarchitecture. Haversian porosity (HP) and tissue mineral density (TMD) have been shown to be among the most relevant determinants of bone quality [Burr (2004)]. HP and TMD describe different aspects of bone microstructure. HP refers to the volume fraction of Havers' and Volkmann's canals (typical diameter of several tens of micrometers) in the bone tissue. TMD measures the degree of mineralization of the bone tissue [Boivin and Meunier (2002); Bouxsein, Boyd, Christiansen, Guldberg, Jepsen, and Müller (2010)]. Spatial variations of HP and TMD in the femoral hip region induce heterogeneity of cortical bone at the organ scale [Bensamoun, Ho Ba Tho, Luu, Gherbezza, and de Belleval (2004); Bensamoun, Gherbezza, de Belleval, and Ho Ba Tho (2004); Yamato, Matsukawa, Otani, Yamazaki, and Nagano (2006); Sasso, Haiat, Yamato, Naili, and Matsukawa (2007, 2008)].

Accurate measures of the spatial variations of HP and TMD can be obtained using synchrotron radiation microtomography [Bousson, Peyrin, Bergot, Hausard, Sautet, and Laredo (2004)]. Recently, detailed experimental data on the spatial variations of HP and TMD in the inferior femoral neck were reported by our group [Sansalone, Naili, Bousson, Bergot, Peyrin, Laredo, and Haiat (2010); Sansalone, Bousson, Naili, Bergot, Peyrin, Laredo, and Haiat (2012)]. In the cross-section of the femoral neck, HP was shown to increase from the periosteum inwards as the dense cortical shell of the femoral neck is progressively replaced by a loose trabecular tissue. TMD was shown to be higher in the periosteal region and to sharply decrease in the inner trabecular region. In the axial direction, TMD decreases from the distal to the proximal part, whereas HP does not show any significant trend.

Spatial variations of bone microstructural properties (such as HP and TMD) make bone a heterogeneous and anisotropic medium at the organ scale. This heterogeneity strongly affects the mechanical response of bone as it was widely documented by studies on the ultrasonic wave propagation [Haiat, Naili, Grimal, Talmant, Desceliers, and Soize (2009); Naili, Vu, Grimal, Talmant, Desceliers, Soize, and Haiat (2010); Haiat, Naili, Vu, Desceliers, and Soize (2011)] and nanoindentation [Yao, Dao, Carnelli, Tai, and Ortiz (2011)]. The complex mechanical behavior of bone can be explained only considering the hierarchical organization of bone at many spatial scales [Rho, Kuhn-Spearing, and Zioupos (1998)]. In this respect, the relevance of modeling approaches capable to account for the specific composition and organization of bone constituents at each scale is apparent [Aoubiza, Crolet, and Meunier (1996); Hellmich, Ulm, and Dormieux (2004); Fritsch and Hellmich (2007); Predoi-Racila and Crolet (2008); Yoon and Cowin (2008b,a); Ghanbaria and Naghdabadi (2009)]. In the line of these papers, the spatial variations of the bone effective elastic coefficients in the cortical neck were studied accounting for the heterogeneous distributions of HP and TMD. Experimental data presented in [Sansalone, Naili, Bousson, Bergot, Peyrin, Laredo, and Haiat (2010); Sansalone, Bousson, Naili, Bergot, Peyrin, Laredo, and Haiat (2012)]—obtained at the scale of several micrometers—were used to estimate the effective elastic coefficients of bone at the scale of the organ using multiscale models based on either asymptotic homogenization [Parnell, Vu, Grimal, and Naili (2012)] or continuum micromechanics [Sansalone, Naili, Bousson, Bergot, Peyrin, Laredo, and Haiat (2010); Sansalone, Bousson, Naili, Bergot, Peyrin, Laredo, and Haiat (2012)]. In particular, these latter papers proposed a three-step homogenization model accounting for the specific microstructure and composition of the bone tissue. In those studies, the effects of the variations of the HP and TMD in the cross section of the femoral neck, as well as the variations of the TMD only along the axis of the femoral neck, were considered. While acknowledging the axial variations of the HP, no relevant de-

pendency of the HP on the axial location was observed. Therefore, effective elastic coefficients of bone were computed assuming HP to be constant in the axial direction. The aim of this paper is to extend and complete those results by investigating in detail the effects of the *combined* actual axial variations of HP and TMD on the effective elastic coefficients of bone at the organ scale and to assess the effects of the above assumptions (constant values of either HP or TMD along the femoral axis) on the estimated elastic coefficients of bone.

This paper is organized as follows. After this introduction, in Sec. 2 we outline the experimental procedure and the data treatment leading to the the spatial variations of HP and TMD. Then, in Sec. 3 we describe the homogenization model used to estimate the elastic coefficients of bone. In Sec. 4 we show and discuss the experimental and numerical results focusing on the effects of the axial variation of HP and TMD on the effective elastic coefficients of bone. Eventually, in Sec. 5 we discuss our results and draw the conclusions of this study opening the way to further research.

2 Materials and methods

In this section we outline the experimental procedure used to acquire the spatial distribution of HP and TMD in a bone sample and the data treatment strategy. More details can be found in [Sansalone, Naili, Bousson, Bergot, Peyrin, Laredo, and Haiat (2010); Sansalone, Bousson, Naili, Bergot, Peyrin, Laredo, and Haiat (2012)].

2.1 Sample preparation

One specimen of human femoral cortical bone from a 79 years old patient was collected during standard hemiarthroplasty for intracapsular hip fracture treatment. The study protocol was approved by our institutional review board. This same specimen was part of the control group used in two earlier studies focusing on bone microstructure [Bousson, Peyrin, Bergot, Hausard, Sautet, and Laredo (2004); Wu, Bergot, Jolivet, Zhou, Laredo, and Bousson (2009)]. The specimen was obtained from the inferior femoral neck because this site is the region of the neck where the cortex is the thickest, due to compression stresses which are mainly transmitted through the inferior neck during ambulation [Werner, Iversen, and Therkildsen (1988)], and therefore provides enough material for an accurate assessment of mineral content. Moreover, in this region of the femoral neck, there is a smooth transition between cortical and trabecular tissue. The bone specimen was fixed in ethanol and embedded in a polyester resin. A parallelepiped sample ($7 \times 7 \times 12$ mm^3) was obtained by two cuts orthogonal to the axis of the bone specimen. The cuts were made (*i*) at the base of the neck and at a right angle to the neck and (*ii*) at the base of

the head, parallel to the first one, to obtain an approximately 6 mm long segment of femoral neck. The edges of the sample were aligned with a cartesian frame whose z axis and (x,y) plane identify the axis and the cross-section of the femoral neck, respectively.

2.2 Synchrotron Radiation Microtomography (SR-μCT)

The parallelepiped sample was imaged using the X-ray microtomography setup developed at the European Synchrotron Radiation Facility (ESRF, Grenoble, France) on the ID19 (topography and high-resolution diffraction) beamline [Salome, Peyrin, Cloetens, Odet, Laval-Jeantet, Baruchel, and Spanne (1999)]. After passing through a monochromator, the X-ray beam energy was tuned to 25 keV. A total of 900 radiographic projections were acquired. Then, the 3-D image was reconstructed using a customized Filtered Back Projection algorithm developed at ESRF. The reconstruction was performed in a volume of interest of $660 \times 660 \times 523$ isotropic voxels (size 10.13 μm). Grayscale levels of the reconstructed image correspond to the linear attenuation of the X-ray through the sample at 25 keV. A typical 2-D cross-section image obtained by SR-μCT is shown in Fig. 1.

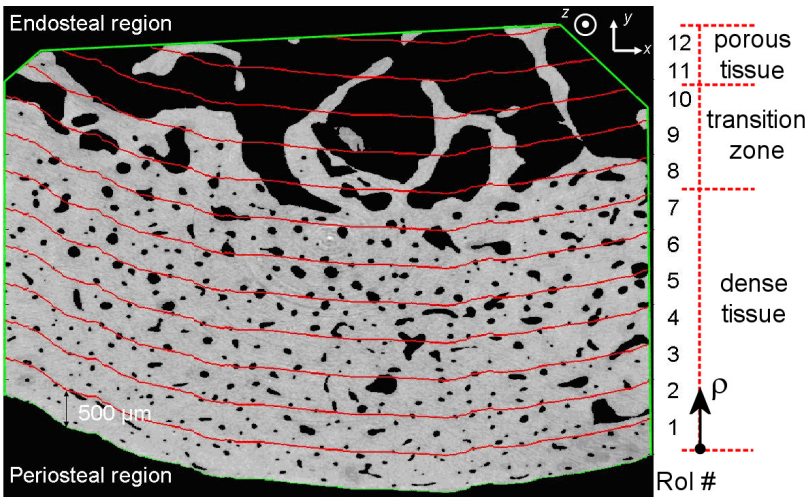

Figure 1: Typical cross-section of the bone sample. Red lines separate the 12 relevant regions of interest (RoIs).

2.3 Image analysis

All the 2-D cross-section images were analyzed to obtain the spatial mapping of the HP and TMD in the bone sample according to the scheme in Fig. 2. We recall here

the main points and refer to [Sansalone, Naili, Bousson, Bergot, Peyrin, Laredo, and Haiat (2010); Sansalone, Bousson, Naili, Bergot, Peyrin, Laredo, and Haiat (2012)] for more details.

The 523 2-D images of cross-sections in the (x,y) plane were labeled from the distal (cross-section ♯1, $z = 0$ mm) to the proximal (cross-section ♯523, $z = 5.3$ mm) part of the femoral neck. Each 2-D image was analyzed using a threshold method to detect the positions of the periosteum and endosteum and to identify the voxels belonging to either the pores or the bone matrix. Stacking the 523 2-D images (Fig. 2(a)), the voxel-wise 3-D volume of the bone sample was reconstructed (Fig. 2(b)). This volume was subdivided in $N_r = 12$ radial regions of interest (RoIs) and $N_z = 10$ slices, see Fig. 2. Roughly speaking, RoIs are 50-pixel thick coaxial cylindrical shells obtained by virtual concentric cuts of the bone sample (corresponding to a RoI thickness of $L_r = 506.5$ μm). Slices collect 50 consecutive cross-sections (corresponding to a slice thickness of $L_z = 506.5$ μm). RoIs were labeled by the discrete radial coordinate ρ, starting from the periosteal region which corresponds to $\rho = 1$ (Fig. 1). Slices were labeled by the discrete axial coordinate ζ, starting from the distal part of the sample which corresponds to $\zeta = 1$. The intersection between a RoI and a slice is a ring segment referred to as Volume of Interest (VoI). A VoI is identified by its discrete coordinates (ρ,ζ).

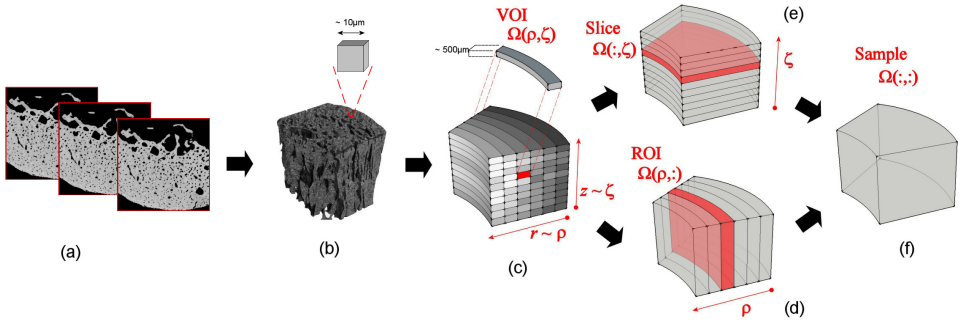

Figure 2: Schematic representation of the sample: (a) stack of 2-D images, (b) 3-D voxel representation (grayscale refer to the TMD level, see text for more details), (c) volume of interest $\Omega(\rho,\zeta)$, (d) radial region of interest $\Omega(\rho,:)$, (e) axial slice $\Omega(:,\zeta)$, and (f) whole sample $\Omega(:,:)$.

Spatial mappings of HP and TMD were computed according to the schemes shown in Fig. 2, namely in VoIs $\Omega(\rho,\zeta)$ (Fig. 2(c)), radial RoIs $\Omega(\rho,:) = \bigcup_\zeta \Omega(\rho,\zeta)$ (Fig. 2(d)), axial slices $\Omega(:,\zeta) = \bigcup_\rho \Omega(\rho,\zeta)$ (Fig. 2(e)), and whole volume $\Omega(:,:)$ = $\bigcup_{\rho,\zeta} \Omega(\rho,\zeta)$ (Fig. 2(f)). In this study, we are only concerned with steps (a)-(d)

of Fig. 2. More precisely, spatial distributions of HP and TMD were computed in VoIs and RoIs only. In each VoI, the HP and TMD were computed by averaging the relevant voxel-wise values taken from the 2-D images. In each VoI, HP was computed as the ratio between the number of voxels belonging to pores and the total number of voxels. In each VoI, TMD was computed by averaging the voxel-wise distribution of TMD, this latter being computed based on the grayscale levels of the image. VoI-wise distribution of HP and TMD were then axially averaged to obtain the average value in each RoI. (Henceforth, axial averages are denoted by $< * >_z$.)

2.4 Statistical analysis

One-way analysis of variance (ANOVA) tests were performed using the MatLab software (The MathWorks Inc, Natick, MA, USA) to evaluate whether HP and TMD had a significant dependence on the axial position.

2.5 Volume fractions of bone constituents

For each VoI, the composition of the bone solid matrix was determined. Also, average compositions in the radial RoIs were determined by using the same averaging procedure as for HP and TMD. At the tissue level, HP provides the volume fraction of the pores. Then, volume fraction of the bone matrix is $1 - \mathrm{HP}$. Bone matrix is mainly made of collagen, mineral and water. (Other bone constituents such as non-collagenous proteins or vasculature are disregarded in our analysis.) Volume fractions of these elementary constituents are denoted f_{col}, f_{HA}, and f_{w}, respectively (with $f_{\mathrm{col}} + f_{\mathrm{HA}} + f_{\mathrm{w}} = 1$), and were computed as in [Sansalone, Naili, Bousson, Bergot, Peyrin, Laredo, and Haiat (2010); Sansalone, Bousson, Naili, Bergot, Peyrin, Laredo, and Haiat (2012)] based on the TMD value previously determined for each VoI. In particular, f_{HA} is estimated as $f_{\mathrm{HA}} = \mathrm{TMD}/\rho_{HA}$, where ρ_{HA} is the mass density of the mineral. Then, f_{col} and f_{w} are estimated through the empirical relation [Raum, Cleveland, Peyrin, and Laugier (2006)]:

$$\frac{f_{\mathrm{col}}}{f_{\mathrm{w}}} = 0.36 + 0.084\, e^{6.7 f_{\mathrm{HA}}}. \tag{1}$$

2.6 Elastic properties of bone constituents

Following [Hellmich, Barthelemy, and Dormieux (2004)], collagen was assumed transversely isotropic and mineral and water were assumed isotropic. Relevant elastic coefficients, taken from [Hellmich, Barthelemy, and Dormieux (2004)], are resumed in Tab. 1. In what follows, the x, y and z axes of the sample are associated with the subscripts 1, 2 and 3 identifying the components of the elasticity tensor.

Table 1: Elastic coefficients of bone constituents [GPa], taken from [Hellmich, Barthelemy, and Dormieux (2004)].

Collagen (transversely isotropic)		
$\mathbb{C}_{\text{col},1111}$	11.7	Coefficients of
$\mathbb{C}_{\text{col},3333}$	17.9	the elastic tensor
$\mathbb{C}_{\text{col},1122}$	5.1	
$\mathbb{C}_{\text{col},1133}$	7.1	
$\mathbb{C}_{\text{col},1313}$	3.3	
Mineral (isotropic)		
K_{HA}	82.6	Bulk modulus
μ_{HA}	44.9	Shear modulus
Water (isotropic)		
K_{w}	2.3	Bulk modulus
μ_{w}	0.0	Shear modulus

3 Model

The spatial distribution of the HP and of the volume fractions of the bone constituents were used as input data in a multiscale model based on continuum micromechanics theory. This approach was initially proposed by Hellmich and coworkers [Hellmich, Ulm, and Dormieux (2004); Hellmich, Barthelemy, and Dormieux (2004)] and further extended by [Sansalone, Naili, Bousson, Bergot, Peyrin, Laredo, and Haiat (2010)] to estimate the effective elastic coefficients of bone at the organ scale.

3.1 Continuum micromechanics

Continuum micromechanics provides estimates of the effective elasticity tensor for materials with microstructure of matrix-inclusion type. We recall here the main ingredients of the theory and refer to [Suquet (1997); Nemat-Nasser and Hori (1999); Zaoui (2002)] for further details. Continuum micromechanics steps from the solution of the elastic problem of an isolated inclusion embedded in an infinitely extended matrix provided by Eshelby in the fifties [Eshelby (1957)]. Eshelby's solution describes the elastic fields (strain, stress) engendered by one ellipsoidal inclusion in an infinite isotropic elastic matrix under homogeneous strain/stress boundary conditions at infinity. Eshelby's solution was further extended to inclusions of different shapes [Suvorov and Dvorak (2002)], including cylinders and penny-shaped cracks [Laws (1985)], and to anisotropic matrices [Laws (1977)]. Moreover, Eshelby's solution for an isolated inclusion served as basis to account

for several inclusions and for multiphase media. Let $\mathbb{C}^{hom}$ be the homogenized elasticity tensor describing the effective elastic properties of a material with microstructure. In continuum micromechanics theory, $\mathbb{C}^{hom}$ reads:

$$\mathbb{C}^{hom} = \sum_r f_r \, \mathbb{c}_r : \mathbb{A}_r \,, \tag{2}$$

where f_r is the volume fraction of phase r ($\sum_r f_r = 1$) and $\mathbb{c}_r$ and $\mathbb{A}_r$ are the elasticity and localization tensors of phase r, respectively. It can be shown that the expression of $\mathbb{A}_r$ reads [Hellmich, Barthelemy, and Dormieux (2004)]:

$$\mathbb{A}_r = \left(\mathbb{I} + \mathbb{P}_r^0 : \left(\mathbb{c}_r - \mathbb{C}^0\right)\right)^{-1} : \left(\sum_s f_s \left(\mathbb{I} + \mathbb{P}_s^0 : \left(\mathbb{c}_s - \mathbb{C}^0\right)\right)^{-1}\right)^{-1}, \tag{3}$$

where $\mathbb{I}$ is the 4th order symmetric identity tensor ($\mathbb{I}_{ijhk} = \frac{1}{2}(\delta_{ih}\delta_{jk} + \delta_{ik}\delta_{jh})$, δ being the Kronecker operator), $\mathbb{C}^0$ is the elasticity tensor of the "effective matrix" (hereafter referred to by superscript "0") where the phases are embedded, and $\mathbb{P}_r^0$ is the Hill tensor of phase/inclusion r embedded in the effective matrix. The expression of the Hill tensor $\mathbb{P}_r^0$ depends on the shape of the inclusions representing the phase r and on the elastic tensor of the surrounding effective matrix. Explicit expressions of the Hill tensor have been developed in some special cases [Suvorov and Dvorak (2002)] but, in general, it has to be computed numerically. The choice of the value of $\mathbb{C}^0$ leads to different estimates of $\mathbb{C}^{hom}$. Among others, two estimates are relevant to our context. The Mori-Tanaka (MC) estimate is well suited to describe the elasticity tensor of a material made of uniformly dispersed inclusions in a homogeneous matrix. In this case, the effective matrix is an actual, well identified phase and therefore $\mathbb{C}^0 = \mathbb{c}_{matrix}$. The Self-Consistent (SC) estimate is well suited for disordered multi-phase media for which no "matrix" phase can be identified, but the material is rather constituted of interpenetrating discontinuous phases [Suquet (1997)]. In this case, the homogenized properties of the effective medium are estimated based on the idea of placing each inhomogeneity in the homogeneous effective medium. Therefore, the matrix is assumed to be the homogenized material itself and $\mathbb{C}^0 = \mathbb{C}^{hom}$. Hereafter, $\mathbb{C}^{hom}_{\text{MT}}$ and $\mathbb{C}^{hom}_{\text{SC}}$ will refer to the MT and SC estimates of $\mathbb{C}^{hom}$, respectively.

3.2 Application to bone tissue

At the organ scale, bone is a heterogenous and anisotropic multiscale material. Heterogeneity depends on the spatial variations of bone physical properties (*e.g.*, TMD and HP). Anisotropy depends on the hierarchical organization of bone microstructure. Between the scale of the organ and the scale of its individual constituents, bone shows many levels of structural organization. Following [Sansalone, Naili,

Bousson, Bergot, Peyrin, Laredo, and Haiat (2010); Sansalone, Bousson, Naili, Bergot, Peyrin, Laredo, and Haiat (2012)], we adopt a simplified representation of bone, considering three scales of representation below the organ scale: the cortical tissue, the ultrastructure and the mineral foam (Fig. 3). At each scale, the type of elastic behavior of the homogenized material results from the elastic behavior and morphology of the constituent phases.

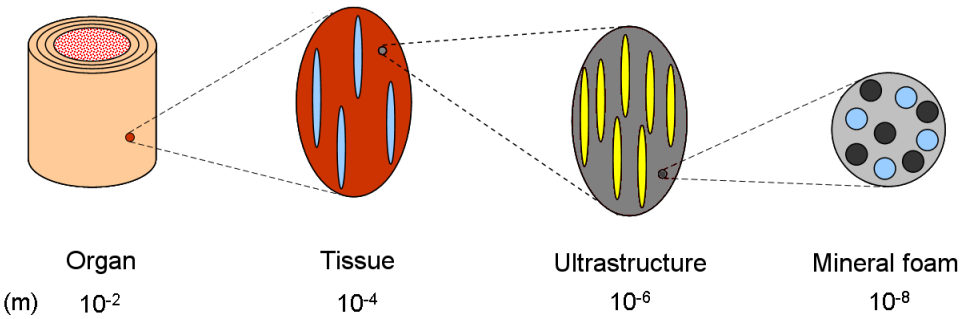

Figure 3: Three-step homogenization model and characteristic length scales.

3.2.1 *Mineral foam*

At the scale of few hundred nanometers, highly disordered hydroxyapatite crystals interpenetrated by water-filled spaces form a mineral foam. The disordered structure observable at this scale [Lees, Prostak, Ingle, and Kjoller (1994)] motivates the use of a Self-Consistent scheme to compute the homogenized properties of the mineral foam [Hellmich, Barthelemy, and Dormieux (2004)]. Lacking precise morphological information, both mineral and pores were considered as spherical particles. Both mineral and water phases were considered as isotropic materials. The corresponding mixture is isotropic. The homogenized elasticity tensor of the mineral foam $\mathbb{C}^{foam}$ was computed iteratively solving Eq. (2) and Eq. (3) after setting $\mathbb{C}^{hom} = \mathbb{C}^0 = \mathbb{C}^{foam}$ and specifying the expressions of the Hill tensor of the mineral and water as for spherical inclusions in an isotropic matrix.

3.2.2 *Ultrastructure*

At the scale of several microns, collagen molecules are embedded in the mineral foam. The elongated form of collagen molecules and the contiguity of the mineral phase motivates the use of a Mori-Tanaka scheme to compute the homogenized properties of the ultrastructure [Hellmich, Barthelemy, and Dormieux (2004)]. According to this scheme, the matrix phase is the (isotropic) mineral foam previously

described and the collagen is modeled as cylindrical inclusions. Collagen was considered as a transversely isotropic material. The mixture obtained is transversely isotropic. The homogenized elasticity tensor of the ultrastructure $\mathbb{C}^{ultra}$ was computed through Eq. (2) and Eq. (3) after setting $\mathbb{C}^{hom} = \mathbb{C}^{ultra}$, $\mathbb{C}^{0} = \mathbb{C}^{foam}$ and specifying the expression of the Hill tensor of the collagen as for cylindrical inclusions in an isotropic matrix.

3.2.3 Cortical tissue

At the scale of several hundred microns, cortical bone tissue is a porous medium made of a solid matrix (the ultrastructure) crossed by the Haversian canals. (We neglect any other geometrical feature related to the osteonal structure.) The pseudo-cylindrical shape of the Haversian canals motivates the use of a Mori-Tanaka scheme to compute the homogenized properties of the cortical tissue [Sansalone, Naili, Bousson, Bergot, Peyrin, Laredo, and Haiat (2010)]. According to this scheme, the matrix phase is the (transversely isotropic) ultrastructure previously described and the Haversian canals are modeled as water filled cylindrical inclusions. The mixture obtained is transversely isotropic. The homogenized elasticity tensor of the tissue $\mathbb{C}^{cort}$ was computed through Eq. (2) and Eq. (3) after setting $\mathbb{C}^{hom} = \mathbb{C}^{cort}$, $\mathbb{C}^{0} = \mathbb{C}^{ultra}$ and specifying the expression of the Hill tensor of the Haversian canals as for cylindrical inclusions in a transversely isotropic matrix.

3.2.4 Volume fractions

The model requires the knowledge of the volume fractions of the bone constituents at each scale. VoI-averaged values of the HP and TMD were used to obtain the average volume fractions in each VoI. The HP is the volume fraction of the pores and $1 - \mathrm{HP}$ is the volume fraction of the bone matrix (ultrastructure) in the tissue. The TMD value is used to compute the composition of the bone matrix (f_{col}, f_{HA}, and f_{w}) as explained in Sec. 2.5. The value of f_{col} is the volume fraction of the collagen inclusions and $f_{\mathrm{HA}} + f_{\mathrm{w}}$ is the volume of the matrix (mineral foam) in the ultrastructure. Eventually, the volume fractions of the mineral and water in the mineral foam are given by $f_{\mathrm{HA}}/(f_{\mathrm{HA}} + f_{\mathrm{w}})$ and $f_{\mathrm{w}}/(f_{\mathrm{HA}} + f_{\mathrm{w}})$, respectively.

4 Results

4.1 Axial variations of HP and TMD

Fig. 4 shows the axial variations of the HP and TMD for 4 relevant RoIs of the bone sample, namely close to the periosteum (RoI ♯1), in the cortical region (RoI ♯5), in the transition region (RoI ♯9) and in the trabecular region (RoI ♯12), see Fig. 1. Thick and thin lines refer to different samplings of the HP and TMD in

the axial directions, respectively. Each point of the thin lines corresponds to a 2-D image obtained by SR-μCT ($\Delta z = 10.13$ μm). Each point of the thick lines refers to the values in one VoI, *i.e.* to the mean over 50 consecutive cross sections ($\Delta z = 506.5$ μm). Error bars on the thick lines depict the corresponding standard deviation. Thick lines provide a reasonable approximation of the fine grain distribution depicted by the thin lines. This justifies to study the spatial variations of the biomechanical properties in the bone sample based on the VoI-wise values.

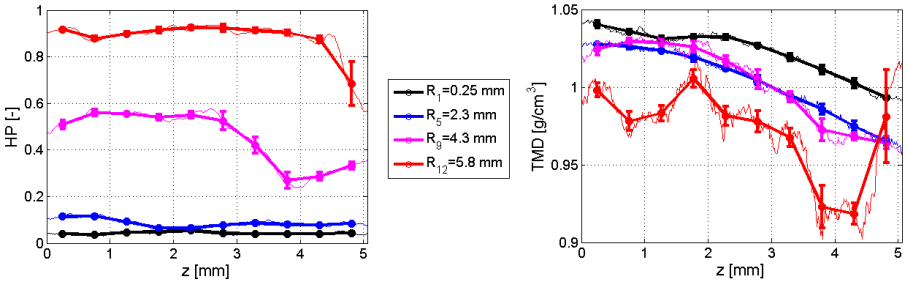

Figure 4: Axial variations of the HP (on the left) and TMD (on the right) at different distances from the periosteum. R_1 corresponds to the periosteal RoI and R_{12} to the endosteal RoI. Thin and thick lines correspond to the 2-D images ($\Delta z = 10.13$ μm) and to the VoIs ($\Delta z = 506.5$ μm), respectively.

The HP does not show any significant trend in the axial direction. This result was confirmed by ANOVA which did not reveal any significant effect of the axial position ($p = 1$, $F = 0$) on the HP.

The TMD does show a significant trend in the axial direction, as confirmed by ANOVA which revealed a significant effect of the axial position ($p < 10^{-5}$, $F = 149$). TMD was found to decrease from the distal to the proximal part. The axial profiles of TMD are quite regular in all the RoIs but in the endosteal one (RoI ♯12), where fluctuations of high amplitude were observed.

The global axial mean and standard divation (computed considering 500 cross sections) of the HP and TMD in the selected four regions of interest are resumed in Tab. 2. From Fig. 4 it is apparent that the dispersion of both HP and TMD is small in the cortical regions, then increases in the transition and endosteal regions. The dispersion of both the HP and TMD is always higher in the endosteal region (RoI ♯12) than in the periosteal region (RoI ♯1). Indeed, the ratio between the global axial dispersions of the HP and TMD in the endosteal and periosteal regions is higher than 10 and smaller than 2, respectively.

Table 2: Global axial means (standard deviations) of the HP and TMD.

RoI ♯	1	5	9	12
HP [−]	0.0428 (0.0061)	0.0856 (0.0176)	0.4545 (0.1141)	0.8830 (0.0753)
TMD [g/cm^3]	1.0225 (0.0149)	1.0032 (0.0214)	1.0028 (0.0254)	0.9714 (0.0298)

4.2 Axial variations of the effective elastic coefficients of bone

The axial variations of HP and TMD affect the effective elastic properties of the bone at the organ scale. In order to elucidate this point, the elastic coefficient $\mathbb{C}^{cort}_{3333}$ of the effective elasticity tensor of bone is plotted in Fig. 5. This coefficient was chosen since it features the stiffness of bone sample along its axis, which corresponds to the main loading direction [Lotz, Cheal, and Hayes (1995)]. Similar results were obtained for the other coefficients of the effective elasticity tensor (data not shown).

Plots in Fig. 5 corresponds to the 4 relevant RoIs identified in the previous section, namely close to the periosteum (RoI ♯1), in the cortical region (RoI ♯5), in the transition region (RoI ♯9) and in the trabecular region (RoI ♯12). In each plot, different scenarios of axial variations of HP and TMD were considered to investigate the relative effects of these parameters on the elastic coefficients of bone. Black lines correspond to the actual axial values of HP and TMD in the z direction and have to be taken as reference. Red lines with empty markers correspond to the actual axial values of TMD and to a constant value of HP equal to its axial average (the mean values of the HP are reported in the first line of Tab. 2). Blue lines with solid markers correspond to the actual axial values of HP and to a constant value of TMD equal to its axial average (the mean values of the TMD are reported in the second line of Tab. 2). Therefore, red and blue lines allow identifying the effects of considering approximate values (axial averages) of HP and TMD, respectively. It can be noticed that the behaviors in the four regions are different. In the periosteal region (RoI ♯1) the red line (average HP) is almost superposed to the black line (reference), whereas the blue line (average TMD) is completely different. This means that close to the periosteum the axial variations of the HP do not really matter while the axial variations of TMD strongly affect the effective elasticity of bone. A similar behavior is also apparent in the cortical RoI ♯5. By contrast, an opposite behavior is apparent close to the endosteum. In the porous bone (RoI ♯12), the blue line is quite close to the black line whereas the red line is not. That means that considering an average value of TMD does not lead to significant errors in estimating

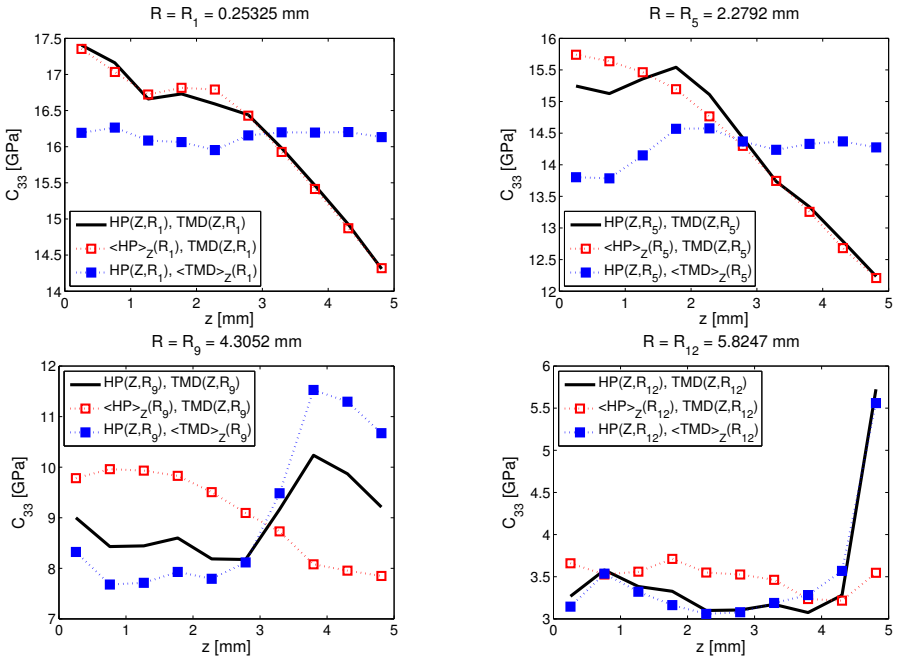

Figure 5: Axial variations of the effective elastic coefficient $\mathbb{C}^{cort}_{3333}$ (denoted C_{33} in the plots) at different distances from the periosteum. Each plot refers to a different RoI identified by its radial coordinate *R*. Black lines: actual axial values of HP and TMD (reference). Red lines with empty markers: actual axial values of TMD and average axial value of HP. Blue lines with solid markers: actual axial values of HP and average axial value of TMD.

the effective elasticity of bone, while axial variations of HP should be taken into account. Eventually, in the transition zone (RoI ♯9) an intermediate behavior can be observed and the elasticity of bone is determined by the combined axial variations of both HP and TMD.

5 Discussion

Both porosity and mineralization of bone tissue, as well as bone microarchitecture, are known to affect bone mechanical properties [Burr (2004); Dong and Guo (2004); van der Linden, Birkenhager-Frenkel, Verhaar, and Weinans (2001)]. Nevertheless, the effects of the anatomical variations of bone microstructural features on the bone elastic properties remain poorly documented. To the best of our knowledge, this paper constitutes the first attempt to estimate the effects of the axial vari-

ations of the Haversian Porosity (HP) and Tissue Mineral Density (TMD) on the bone elastic properties in the femoral neck. The salient findings of this study are the following:

- HP does vary along the axis of the femoral neck;
- HP values do not show any global trend along the axis of the femoral neck;
- HP axial variations strongly affect the bone effective elastic coefficients in porous bone;
- TMD axial variations strongly affect the bone effective elastic coefficients in dense bone;
- axial variations of both HP and TMD should be considered to provide accurate estimates of the bone effective elastic properties.

The strategy followed in this paper was twofold. First, we performed a detailed analysis of the spatial variations of the HP and TMD in the inferior femoral neck based on high-resolution 3-D images obtained by Synchrotron Radiation Microtomography (SR-μCT). Then, we investigated the effects of these variations on the effective elastic properties of bone using a multiscale homogenization model based on continuum micromechanics. This approach was first used in [Sansalone, Naili, Bousson, Bergot, Peyrin, Laredo, and Haiat (2010)] and further developed in [Sansalone, Bousson, Naili, Bergot, Peyrin, Laredo, and Haiat (2012)]. In these studies, the focus was set on the radial variations of the HP and TMD and on the axial variation of the TMD only within the femoral neck. One-way analysis of variance (ANOVA) having shown no relevant dependency of HP on the axial location, HP was taken constant and equal to its axial average in each RoI. Under this assumption, it was shown that the axial variation of the TMD affects the axial variations of the elastic coefficients of bone. While acknowledging the axial variations of the HP, the effects of these variations on the effective elastic properties of bone were not investigated.

The main goal of this paper was to fill this gap and to make a further step in understanding the relationships between bone elasticity and anatomical variations of bone microstructure accounting for the *actual* variations of both the HP and TMD along the femoral axis. To this aim, the actual radial-axial mapping of the HP and TMD was first determined in the bone sample (Sec. 4.1). Then, the effective elastic coefficients of the bone were estimated based on these data (Sec. 4.2). The axial position was found to significantly affect the TMD but not the HP. TMD was found to decrease from the distal to the proximal part of the sample in all the

RoIs (Fig. 4(B)). HP was found to significantly vary along the axis of the sample (Fig. 4(A)). However, the axial profile of the HP did not show any global trend but rather random variations. These variations may affect the actual elastic properties of bone and induce errors when considering a constant value of HP as it was done in previous studies [Sansalone, Naili, Bousson, Bergot, Peyrin, Laredo, and Haiat (2010); Sansalone, Bousson, Naili, Bergot, Peyrin, Laredo, and Haiat (2012)]. In order to elucidate this point, we considered different axial distributions of HP and TMD which were considered either variable (actual distributions as obtained by the analysis of the SR-μCT images) or constant (axial averages in each RoI) in the axial direction. (In the radial direction the RoI-wise actual distribution was always considered.) We compared the bone effective elastic coefficients obtained in each scenario to highlight the effects of considering axially-constant values of these parameters. Our results show that the errors introduced by considering axial averages of either HP or TMD are relevant and the actual axial variations of both parameters should be taken into account to provide accurate estimates of bone effective elastic properties. The axial variations of the bone effective elastic coefficients are dominated by either TMD or HP in the periosteal and endosteal regions, respectively. In particular, axial variations of TMD are more relevant in the cortical, dense tissue (Fig. 5.(A,B)) whereas axial variations of HP are more relevant in the trabecular, porous tissue (Fig. 5.(D)). Moreover, both of them are relevant in the transition zone between cortical and trabecular tissue (Fig. 5.(C)).

It is interesting to relate these conclusions to the values of the dispersions of the HP and TMD reported in Tab. 2. Indeed, the errors induced by considering average values of either HP and TMD in estimating the elastic coefficients of bone are not evenly correlated to the dispersions of the HP and TMD values. On the one side, the ratio between the standard deviation and the mean of the HP is quite small in each RoI (several percents to a few ten percents). The error induced by considering the average value of HP instead of its actual values throughout the axial direction on the estimated elastic coefficients of bone remains limited as long as the volume fraction of the HP is small (periosteal and cortical regions). The error increases as the volume fraction of the HP increases and becomes important for HP values higher than a few ten percents. On the other side, the ratio between the standard deviation and the mean of the TMD is quite high in each RoI (few percents). The error induced by considering the average value of TMD instead of its actual highly dispersed values throughout the axial direction on the estimated elastic coefficients of bone remains limited as long as the volume fraction of the bone matrix $(1-\mathrm{HP})$ is small (endosteal region). The error increases rapidly as the volume fraction of the bone matrix increases (transition and cortical regions) highlighting the importance of the TMD in determining the elastic properties of bone.

Model predictions were compared with available experimental data. The first two steps of the micromechanical model have been validated against independent experimental sets [Hellmich and Ulm (2002); Hellmich, Barthelemy, and Dormieux (2004); Fritsch and Hellmich (2007)], which lets us expect a reliable prediction of anisotropic and inhomogeneous elastic properties obtained from SR-μCT data. For validation of the model at the organ scale (third step of the model), we refer to [Guo (2001)] who provides an extensive review of experimental data on both cortical and trabecular bone. Model predictions in the cortical regions compare well with published experimental work on cortical bone (see, *e.g.*, [Dong and Guo (2004)]). Experimental validation of model predictions in the trabecular regions is not straightforward. Indeed, the elastic properties of the trabecular bone strongly depend on its microstructural organization. This organization is disregarded in this study and therefore direct comparison of our results with trabecular bone data is more difficult. Moreover, it should be kept in mind that direct comparison of the elastic properties predicted by the model with experimental data is only meaningful with respect to bone samples having the same microstructural organization, biomechanical properties (namely, HP and TMD) and geometrical size (around 500 micrometers).

This multi-faceted behavior corresponds to the different types of bone tissue which can be found in the femoral neck. In this study, cortical bone was defined as having HP lower than 15% [Dong and Guo (2004)] and is located at a distance lower than 3.5 mm from the periosteum for the sample considered herein. Trabecular bone was defined as having HP higher than 75% [Haiat, Padilla, Peyrin, and Laugier (2007)] and was located at a distance higher than 4.8 mm from the periosteum. The intermediate region corresponded to the transition zone. The definition of these three zones allowed identifying zone-specific relationships between microstructural features (HP and TMD) and effective elastic properties of bone.

This study provided new insights on the determinants of bone effective elasticity. However, some assumptions were made in obtaining these results which need further investigation. First, we were concerned with only the inferior part of the femoral neck. This part of the femoral neck supports most of the loads during normal walking [Voo, Armand, and Kleinberger (2004)]. However, aiming at establishing the global risk of fracture, the whole femoral neck should be considered [Manske, Liu-Ambrose, Cooper, Kontulainen, Guy, Forster, and McKay (2008)]. Actually, bone fractures often initiate in the thinner superior cortex, especially in case of sideways falls [de Bakker, Manske, Ebacher, Oxland, Cripton, and Guy (2009)]. Moreover, the axial length of the sample considered in this analysis is relatively small. Analysis of longer samples might improve this study. For instance, random axial variations of the HP were observed in this sample. However, global

trends may appear analyzing longer samples. Furthermore, this study considered only one sample and therefore it does not allow to estimate the effects of aging or health conditions which are well known to affect bone mechanical properties [Mayhew, Thomas, Clement, Loveridge, Beck, Bonfield, Burgoyne, and Reeve (2005); Poole, Mayhew, Rose, Brown, Bearcroft, Loveridge, and Reeve (2010)].

Second, we assumed a simplistic representation of the hierarchical structure of bone. In this study, we only considered three scales (mineral foam, ultrastructure and tissue) below the organ scale. However, bone structure is much more complex and several additional levels exist which are not taken into account in this study. In particular, we neglected many issues related to the osteonal structure, such as the presence of lamellae with different collagen orientation, Volkmann's canals and interstitial tissue. Moreover, we adopted the same geometrical model for the pores in the cortical and trabecular tissue. Indeed, Haversian canals running in the cortical tissue are well represented by axial cylinders. However, resorption cavities of the trabecular tissue have quite irregular shape and are hardly approximated by axial cylinders. All these issues may affect the conclusions of this study, namely with respect to the trabecular tissue, and have to be taken into account to provide accurate estimates of bone elasticity. There exist at the least two directions to improve the model proposed in this study. On the one side, guidelines to improve the multi-scale description of bone can be obtained from other models taking into account some or several levels of the bone hierarchical structure [Fritsch and Hellmich (2007); Yoon and Cowin (2008b,a); Sansalone, Lemaire, and Naili (2009); Ghanbaria and Naghdabadi (2009)]. On the other side, a more detailed analysis of the 3-D representation of bone obtained by SR-μCT will provide accurate information on the morphology and organization of bone porosity and other microstructural features.

Another issue concerns the spatial heterogeneity of HP and TMD which were assumed to be homogeneous in each VoI. For sake of simplicity and being concerned with a small part of the femoral neck, we assumed that bone properties are homogeneous in the hoop direction. However, the reliability of this assumption needs further investigation. Moreover, TMD raises a similar issue also in the axial and radial directions. As it is apparent from Fig. 1 and Fig. 4(B), TMD is heterogeneous at the tissue scale in both the radial and axial directions. The effects of this heterogeneity were disregarded in this study and TMD was considered homogeneous within each VoI. This assumption was introduced to comply with the theory underlying the continuum micromechanics model which requires having a homogeneous matrix embedding the inclusions (in here, the cylindrical pores). Further work is required to overcome this limitation and to include the effect of TMD heterogeneity on the homogenized properties of bone. However, homogeneity of the TMD within the VoI seems not to be a major limitation of the approach. Indeed,

TMD is very heterogeneous at the scale of tens of micrometers, but it seems not to change dramatically in time and space at the millimeter scale. Several arguments supporting this idea can be found in [Hellmich, Kober, and Erdmann (2008); Malandrino, Fritsch, Lahayne, Kropik, Redl, Noailly, Lacroix, and Hellmich (2012)] and references therein.

References

Aoubiza, B.; Crolet, J.; Meunier, A. (1996): On the mechanical characterization of compact bone structure using the homogenization theory. *J. Biomech.*, vol. 29, no. 12, pp. 1539–1547.

Bensamoun, S.; Gherbezza, J.-M.; de Belleval, J.-F.; Ho Ba Tho, M.-C. (2004): Transmission scanning acoustic imaging of human cortical bone and relation with the microstructure. *Clinical Biomechanics*, vol. 19, pp. 639–647.

Bensamoun, S.; Ho Ba Tho, M.-C.; Luu, S.; Gherbezza, J.-M.; de Belleval, J.-F. (2004): Spatial distribution of acoustic and elastic properties of human femoral cortical bone. *J. Biomech.*, vol. 37, pp. 503–510.

Boivin, G.; Meunier, P. (2002): The degree of mineralization of bone tissue measured by computerized quantitative contact microradiography. *Calcif. Tissue Int.*, vol. 70, no. 6, pp. 503–511.

Bousson, V.; Peyrin, F.; Bergot, C.; Hausard, M.; Sautet, A.; Laredo, J. (2004): Cortical bone in the human femoral neck: three-dimensional appearance and porosity using synchrotron radiation. *J. Bone Miner. Res.*, vol. 19, no. 5, pp. 794–801.

Bouxsein, M.; Boyd, S.; Christiansen, B.; Guldberg, R.; Jepsen, K.; Müller, R. (2010): Guidelines for assessment of bone microstructure in rodents using micro-computed tomography. *J. Bone Miner. Res.*, vol. 25, no. 7, pp. 1468–1486.

Burr, D. (2004): Bone quality: understanding what matters. *J. Musculoskelet. Neuronal Interact.*, vol. 4, no. 2, pp. 184–186.

de Bakker, A.; Manske, S.; Ebacher, V.; Oxland, T.; Cripton, P.; Guy, P. (2009): During sideways falls proximal femur fractures initiate in the superolateral cortex: evidence from high-speed video of simulated fractures. *J. Biomech.*, vol. 42, no. 12, pp. 1917–1925.

Dong, X. N.; Guo, X. E. (2004): The dependence of transversely isotropic elasticity of human femoral cortical bone on porosity. *J. Biomech.*, vol. 37, no. 8, pp. 1281–1287.

Eshelby, J. (1957): The determination of the elastic field of an ellipsoidal inclusion, and related problems. *Proc. R. Soc. London, Ser. A*, vol. 241, pp. 376–396.

Fritsch, A.; Hellmich, C. (2007): 'Universal' microstructural patterns in cortical and trabecular, extracellular and extravascular bone materials: micromechanics-based prediction of anisotropic elasticity. *J. Theor. Biol.*, vol. 244, pp. 597–620.

Ghanbaria, J.; Naghdabadi, R. (2009): Nonlinear hierarchical multiscale modeling of cortical bone considering its nanoscale microstructure. *J. Biomech.*, vol. 42, no. 10, pp. 1560–1565.

Guo, X. (2001): Mechanical properties of cortical bone and cancellous tissue. In Cowin, S.(Ed): *Bone Mechanics Handbook*, chapter 10, pp. 10.1–10.23. CRC Press, Boca raton, FL, USA.

Haiat, G.; Naili, S.; Grimal, Q.; Talmant, M.; Desceliers, C.; Soize, C. (2009): Influence of a gradient of material properties on ultrasonic wave propagation in cortical bone: Application to axial transmission. *J. Acoust. Soc. Am.*, vol. 125, no. 6, pp. 4043–4052.

Haiat, G.; Naili, S.; Vu, M.-B.; Desceliers, C.; Soize, C. (2011): Equivalent contributing depth investigated by a lateral wave with axial transmission in heterogeneous viscoelastic cortical bone. *J. Acoust. Soc. Am.*, vol. 129, no. 4, pp. EL114–EL120.

Haiat, G.; Padilla, F.; Peyrin, F.; Laugier, P. (2007): Variation of ultrasonic parameters with microstructure and material properties of trabecular bone: a 3-d model simulation. *J. Bone Miner. Res.*, vol. 22, no. 5, pp. 665–674.

Hellmich, C.; Barthelemy, J.; Dormieux, L. (2004): Mineral-collagen interactions in elasticity of bone ultrastructure - a continuum micromechanics approach. *Eur. J. Mech., A Solids*, vol. 23, pp. 783–810.

Hellmich, C.; Kober, C.; Erdmann, B. (2008): Micromechanics-based conversion of ct data into anisotropic elasticity tensors, applied to fe simulations of a mandible. *Ann. Biomed. Eng.*, vol. 36, no. 1, pp. 108–122.

Hellmich, C.; Ulm, F. (2002): Micromechanical model for ultrastructural stiffness of mineralized tissues. *J. Eng. Mech.*, vol. 128, no. 8, pp. 898–908.

Hellmich, C.; Ulm, F.-J.; Dormieux, L. (2004): Can the diverse elastic properties of trabecular and cortical bone be attributed to only a few tissue-independent phase properties and their interactions? *Biomech. Model. Mechanobiol.*, vol. 2, pp. 219–238.

Laws, N. (1977): The determination of stress and strain concentrations at an ellipsoidal inclusion in an anisotropic material. *Journal of Elasticity*, vol. 7, no. 1, pp. 91–97.

Laws, N. (1985): A note on penny-shaped cracks in transversely isotropic materials. *Mechanics of Materials*, vol. 4, no. 2, pp. 209–212.

Lees, S.; Prostak, K.; Ingle, V.; Kjoller, K. (1994): The loci of mineral in turkey leg tendon as seen by atomic force microscope and electron microscopy. *Calcified Tissue International*, vol. 55, no. 3, pp. 180–189.

Lotz, J.; Cheal, E.; Hayes, W. (1995): Stress distributions within the proximal femur during gait and falls: implications for osteoporotic fracture. *Osteoporos. Int.*, vol. 5, no. 4, pp. 252–261.

Malandrino, A.; Fritsch, A.; Lahayne, O.; Kropik, K.; Redl, H.; Noailly, J.; Lacroix, D.; Hellmich, C. (2012): Anisotropic tissue elasticity in human lumbar vertebra, by means of a coupled ultrasound-micromechanics approach. *Mat. Lett.*, pp. 154–158.

Manske, S.; Liu-Ambrose, T.; Cooper, D.; Kontulainen, S.; Guy, P.; Forster, B.; McKay, H. (2008): Cortical and trabecular bone in the femoral neck both contribute to proximal femur failure load prediction. *Osteop. Int.*, vol. 20, no. 3, pp. 445–453.

Mayhew, P.; Thomas, C.; Clement, J.; Loveridge, N.; Beck, T.; Bonfield, W.; Burgoyne, C.; Reeve, J. (2005): Relation between age, femoral neck cortical stability, and hip fracture risk. *Lancet*, vol. 366, pp. 129–135.

Naili, S.; Vu, M.; Grimal, Q.; Talmant, M.; Desceliers, C.; Soize, C.; Haiat, G. (2010): Influence of viscoelastic and viscous absorption on ultrasonic wave propagation in cortical bone: Application to axial transmission. *J. Acoust. Soc. Am.*, vol. 127, no. 4, pp. 2622–2634.

Nemat-Nasser, S.; Hori, M. (1999): *Micromechanics: Overall properties of heterogeneous materials*. Applied Mathematics and Mechanics. North-Holland, Elsevier Science, Amsterdam, The Netherlands, 2nd edition.

Parnell, W.; Vu, M.; Grimal, Q.; Naili, S. (2012): Analytical methods to determine the effective mesoscopic and macroscopic elastic properties of cortical bone. *Biomech. Model. Mechanobiol.*, vol. 11, pp. 883–901.

Poole, K.; Mayhew, P.; Rose, C.; Brown, J.; Bearcroft, P.; Loveridge, N.; Reeve, J. (2010): Changing structure of the femoral neck across the adult female lifespan. *J. Bone Miner. Res.*, vol. 25, pp. 482–491.

Predoi-Racila, M.; Crolet, J. M. (2008): Human cortical bone: the sinupros model. *Comput. Methods Biomech. Biomed. Engin.*, vol. 11, no. 2, pp. 169–187.

Raum, K.; Cleveland, R.; Peyrin, F.; Laugier, P. (2006): Derivation of elastic stiffness from site-matched mineral density and acoustic impedance maps. *Phys. Med. Biol.*, vol. 51, no. 3, pp. 747–758.

Rho, J.-Y.; Kuhn-Spearing, L.; Zioupos, P. (1998): Mechanical properties and the hierarchical structure of bone. *Medical Engineering & Physics*, vol. 20, pp. 92–102.

Salome, M.; Peyrin, F.; Cloetens, P.; Odet, C.; Laval-Jeantet, A. M.; Baruchel, J.; Spanne, P. (1999): A synchrotron radiation microtomography system for the analysis of trabecular bone samples. *Med. Phys.*, vol. 26, no. 10, pp. 2194–2204.

Sansalone, V.; Bousson, V.; Naili, S.; Bergot, C.; Peyrin, F.; Laredo, J.; Haiat, G. (2012): Anatomical distribution of the degree of mineralization of bone tissue in human femoral neck: Impact on biomechanical properties. *Bone*, vol. 50, no. 4, pp. 876–884.

Sansalone, V.; Lemaire, T.; Naili, S. (2009): Variational homogenization for modeling fibrillar structures in bone. *Mech. Res. Comm.*, vol. 36, no. 2, pp. 265–273.

Sansalone, V.; Naili, S.; Bousson, V.; Bergot, C.; Peyrin, F.; Laredo, J.; Haiat, G. (2010): Determination of the heterogeneous anisotropic elastic properties of human femoral bone: from nanoscopic to organ scale. *J. Biomech.*, vol. 43, no. 10, pp. 1857–1863.

Sasso, M.; Haiat, G.; Yamato, Y.; Naili, S.; Matsukawa, M. (2007): Frequency dependence of ultrasonic attenuation in bovine cortical bone: an in vitro study. *Ultrasound Med. Biol.*, vol. 33, no. 12, pp. 1933–1942.

Sasso, M.; Haiat, G.; Yamato, Y.; Naili, S.; Matsukawa, M. (2008): Dependence of ultrasonic attenuation on bone mass and microstructure in bovine cortical bone. *J. Biomech.*, vol. 41, no. 2, pp. 347–355.

Suquet, P. (1997): *Continuum Micromechanics*, volume 377 of *CISM Lecture Notes*. Springer-Verlag, Wien, Austria.

Suvorov, A.; Dvorak, G. (2002): Rate form of the Eshelby and Hill tensors. *International Journal of Solids and Structures*, vol. 39, no. 21, pp. 5659–5678.

van der Linden, J.; Birkenhager-Frenkel, D.; Verhaar, J.; Weinans, H. (2001): Trabecular bone's mechanical properties are affected by its non-uniform mineral distribution. *J. Biomech.*, vol. 34, pp. 1573–1580.

Voo, L.; Armand, M.; Kleinberger, M. (2004): Stress fracture risk analysis of the human femur based on computational biomechanics. *Johns Hopkins APL Tech. Dig.*, vol. 25, pp. 223–230.

Werner, C.; Iversen, B. F.; Therkildsen, M. H. (1988): Contribution of the trabecular component to mechanical strength and bone mineral content of the femoral neck. An experimental study on cadaver bones. *Scand. J. Clin. Lab. Invest.*, vol. 48, no. 5, pp. 457–460.

Wu, Y.; Bergot, C.; Jolivet, E.; Zhou, L.; Laredo, J.; Bousson, V. (2009): Cortical bone mineralization differences between hip-fractured females and controls. A microradiographic study. *Bone*, vol. 45, no. 2, pp. 207–212.

Yamato, Y.; Matsukawa, M.; Otani, T.; Yamazaki, K.; Nagano, A. (2006): Distribution of longitudinal wave properties in bovine cortical bone in vitro. *Ultrasonics*, vol. 44, no. Suppl 1, pp. e233–e237.

Yao, H.; Dao, M.; Carnelli, D.; Tai, K.; Ortiz, C. (2011): Size-dependent heterogeneity benefits the mechanical performance of bone. *J. Mech. Phys. Solids*, vol. 59, pp. 64–74.

Yoon, Y. J.; Cowin, S. C. (2008): An estimate of anisotropic poroelastic constants of an osteon. *Biomechan. Model. Mechanobiol.*, vol. 7, no. 1, pp. 13–26.

Yoon, Y. J.; Cowin, S. C. (2008): The estimated elastic constants for a single bone osteonal lamella. *Biomechan. Model. Mechanobiol.*, vol. 7, no. 1, pp. 1–11.

Zaoui, A. (2002): Continuum micromechanics: Survey. *Journal of Engineering Mechanics (ASCE)*, vol. 128, no. 8, pp. 808–816.